PTA/07-47

A survey of one-loop electroweak supersymmetric effects in stop-antistop production at LHC

M. Beccaria[a,b], G. Macorini[c,d], L. Panizzi[c,d], F.M. Renard[h] and C. Verzegnassi[c,d]

[a] *Dipartimento di Fisica, Università del Salento, Italy*

[b] *INFN, Sezione di Lecce, Italy*

[c] *Dipartimento di Fisica Teorica, Università di Trieste, Italy*

[d] *INFN, Sezione di Trieste, Italy*

[h] *Laboratoire de Physique Théorique et Astroparticules,*

Université Montpellier II, France

Abstract

We have computed the one-loop electroweak expression of $\widetilde{t}_a \widetilde{t}_b^*$ production from initial state gluons at LHC for the lighter diagonal and for non diagonal pairs in the Minimal Supersymmetric Standard Model. Our results are shown for a choice of ten SUSY benchmark points corresponding to a large variety of parameters values. The possibility of determining sizeable supersymmetric effects in special observables is discussed.

PACS numbers: 12.15.Lk,13.75.Cs,14.70.Dj,14.80.Ly

I. INTRODUCTION

If Supersymmetry exists, and the super particles masses are not all unfairly large, LHC will be able to produce at least a fraction of these new creatures. In particular, the expected values of the cross sections for squark-antisquark pairs production should allow their relatively quick identification. This might be particularly true for the case of final stops, that are supposed to be the lightest squarks in the available theoretical framework of the Minimal Supersymmetric Standard Model (MSSM). Not surprisingly, two calculations of stop-antistop production already exist, one for diagonal [1] and one for non diagonal [2] production. Both calculations include the NLO QCD effect, only relevant for diagonal production, and remain at Born level for what concerns the electroweak contribution. As stressed in [1], the dependence on the various SUSY parameters for diagonal production is in this way limited to the masses of the two produced stops, conventionally defined as $\widetilde{t}_1$ (the lighter one) and $\widetilde{t}_2$. Quoting [1], all the remaining parameters "*affect only the higher order corrections and are not relevant at leading order*". For the non diagonal production,the cross section is so small at leading order [2] that a Born approximation, where in principle also the stop mixing angle appears, seems totally satisfactory. Note that the calculation of [2] is done for the electroweak s-channel Born diagram with Z exchange, whose value turns out to be (surprisingly) possibly larger that that of the (kinematically suppressed) NLO QCD diagrams. The aim of this paper is that of investigating whether the electroweak one-loop contributions could be relevant for diagonal and non diagonal production. More realistically, we shall limit our investigation to those cases where this term could have a certain possible relevance. In particular, we shall consider for the diagonal case the one-loop corrections to the lighter $\widetilde{t}_1\,\widetilde{t}_1^*$ pair production from initial state gluons, largely dominant at LHC. For initial state quark-antiquark and for heavy $\widetilde{t}_2\,\widetilde{t}_2^*$ pair production the expected values of the rates are already so small at Born level [1] that a NLO calculation does not seem motivated. On the contrary, for non diagonal production, the electroweak one-loop contribution to the gluon initiated process, that is vanishing at tree level, has never been computed and, although expected to be very small, might turn out to be competitive with the tree level quark initiated Z exchange of [2]. Our working assumption will be that in a not too far future an integrated luminosity close to the $100\,\mathrm{fb}^{-1}$ limit will be available. This might enable, via a dedicated experimental effort, the detection of *small* supersymmetric effects whose size will be shown

and discussed in this paper. To make our analysis of more immediate possible interest, we have considered a set of ten typical Supersymmetric *benchmark points* commonly used by the LHC ATLAS and CMS groups [4]. A more general investigation would be though easily performable. Our analysis is performed in the following way. Section 2 contains the kinematical description of the process and the various Supersymmetric adopted conventions and notations. In Section 3 the one-loop treatment is quickly presented, with a short discussion on the cancellations of infinities, a detailed verification of the important reproduction of the approximate asymptotic logarithmic Sudakov expansion by the complete one-loop calculation and a short description of the (soft) QED radiation treatment. Section 4 contains the numerical results for the chosen observable quantities and a short final discussion is given in Section 5.

II. THE KINEMATICS OF $g\,g \to \widetilde{t}_a\,\widetilde{t}_b^*$

We consider the process initiated by 2 gluons producing a stop-antistop pair. Physical (mixed) stops and antistops are denoted as $\widetilde{t}_a$, and $\widetilde{t}_b^*$, with a, b running over 1 and 2. They are obtained from the chirality states $\widetilde{t}_i$, $i = 1, 2$ standing for L,R as

$$\widetilde{t}_a = R_{ai}\widetilde{t}_i \tag{1}$$

explicitly

$$\widetilde{t}_1 = \cos\theta_t\widetilde{t}_L + \sin\theta_t\widetilde{t}_R \qquad \widetilde{t}_2 = -\sin\theta_t\widetilde{t}_L + \cos\theta_t\widetilde{t}_R \tag{2}$$

The momenta, polarization vectors and helicities are defined by

$$g(p_g, \epsilon(\lambda_g)) + g(p'_g, \epsilon'(\lambda'_g)) \to \widetilde{t}_a(p_a) + \widetilde{t}_b^*(p_b) \tag{3}$$

The gluon polarization vectors depend on the helicities as

$$\epsilon(g) = \left(0; \frac{-\lambda_g}{\sqrt{2}}, -\frac{i}{\sqrt{2}}, 0\right) \qquad \epsilon'(g) = \left(0; \frac{\lambda'_g}{\sqrt{2}}, -\frac{i}{\sqrt{2}}, 0\right) \tag{4}$$

We use also the kinematical variables

$$s = (p_g + p'_g)^2 = (p_a + p_b)^2 \quad , u = (p_g - p_b)^2 = (p'_g - p_a)^2 \quad , t = (p_g - p_a)^2 = (p'_g - p_b)^2 \tag{5}$$

with

$$p_g = \frac{\sqrt{s}}{2}(1;0,0,1) \qquad p'_g = \frac{\sqrt{s}}{2}(1;0,0,-1) \tag{6}$$

$$p_a = (E_a; p\sin\theta, 0, p\cos\theta) \qquad p_b = (E_b; -p\sin\theta, 0, -p\cos\theta) \tag{7}$$

$$E_a = \frac{s+m_a^2-m_b^2}{2\sqrt{s}} \quad E_b = \frac{s+m_b^2-m_a^2}{2\sqrt{s}} \quad p = \sqrt{E_a^2-m_a^2} \quad \beta = \frac{2p}{\sqrt{s}} \tag{8}$$

The helicity amplitudes F_{λ_g,λ'_g}, computed from the Feynman diagrams listed in the next Section using the polarization vectors of Eq. (4), will appear with various combinations of colors of the external particles. Firstly, one can write the color structure in the form

$$\begin{aligned} F_{\lambda_g,\lambda'_g} \;=\; \{\; & F^1_{\lambda_g,\lambda'_g}[if_{ijl}(\frac{\lambda^l}{2})] + F^2_{\lambda_g,\lambda'_g}[\frac{1}{3}\delta_{ij} + d_{ijl}(\frac{\lambda^l}{2})] \\ & + F^3_{\lambda_g,\lambda'_g}[(\frac{\lambda^i\lambda^j}{4})] + F^4_{\lambda_g,\lambda'_g}[(\frac{\lambda^j\lambda^i}{4})] + F^5[I]\;\}_{\alpha\beta} \end{aligned} \tag{9}$$

where i,j running from 1 to 8 refer to the gluon colors and α,β running from 1 to 3 refer to stop and antistop colors.

The polarized cross sections of the process $g\,g \to \widetilde{t}_a\,\widetilde{t}^*_b$ (averaged over initial and summed over final colors) read

$$\frac{d\sigma(\lambda_g,\lambda'_g)}{d\cos\theta} = \frac{\beta}{2048\pi s}\sum_{col}|F_{\lambda_g,\lambda'_g}|^2 \tag{10}$$

and the unpolarized cross section is

$$\frac{d\sigma}{d\cos\theta} = \frac{1}{4}\sum_{\lambda_g,\lambda'_g}\frac{d\sigma(\lambda_g,\lambda'_g)}{d\cos\theta} \tag{11}$$

The color summation can be explicitly written as

$$\begin{aligned} \sum_{col(ij\alpha\beta)}|F_{\lambda_g,\lambda'_g}|^2 \;=\; & 12|F^1_{\lambda_g,\lambda'_g}|^2 + \frac{28}{3}|F^2_{\lambda_g,\lambda'_g}|^2 + \frac{16}{3}(|F^3_{\lambda_g,\lambda'_g}|^2 + |F^4_{\lambda_g,\lambda'_g}|^2) \\ & + 12(F^1_{\lambda_g,\lambda'_g}F^3_{\lambda_g,\lambda'_g} - F^1_{\lambda_g,\lambda'_g}F^4_{\lambda_g,\lambda'_g}) + \frac{28}{3}(F^2_{\lambda_g,\lambda'_g}F^3_{\lambda_g,\lambda'_g} + F^2_{\lambda_g,\lambda'_g}F^4_{\lambda_g,\lambda'_g}) \\ & - \frac{4}{3}F^3_{\lambda_g,\lambda'_g}F^4_{\lambda_g,\lambda'_g} + 16F^2_{\lambda_g,\lambda'_g}F^5_{\lambda_g,\lambda'_g} + 8(F^3_{\lambda_g,\lambda'_g}F^5_{\lambda_g,\lambda'_g} + F^4_{\lambda_g,\lambda'_g}F^5_{\lambda_g,\lambda'_g}) \\ & + 24|F^5_{\lambda_g,\lambda'_g}|^2 \end{aligned} \tag{12}$$

The Born terms

The Born terms exist only for "diagonal" stop-antistop pairs ($a \equiv b$). They are given by 4 diagrams shown in Fig (1):

$$A^{Born} = A^{Born\ A} + A^{Born\ A'} + A^{Born\ B} + A^{Born\ C} \tag{13}$$

(A) s-channel gluon exchange:

$$A_{ab}^{Born\ A} = [if^{ijl}\frac{\lambda^l}{2}](4\pi\alpha_s)(\epsilon.\epsilon')\frac{t-u}{s}\delta_{ab} \tag{14}$$

(A') 4-leg $g^i g^j \widetilde{t}_a \widetilde{\bar{t}}_a$ diagram:

$$A_{ab}^{Born\ A'} = [\frac{1}{3}\delta_{ij} + d^{ijl}\frac{\lambda^l}{2}](4\pi\alpha_s)(\epsilon.\epsilon')\delta_{ab} \tag{15}$$

(B) stop exchange in the t-channel:

$$A_{ab}^{Born\ B} = -\frac{16\pi\alpha_s}{t-m_{\widetilde{t}_a}^2}\ [\frac{\lambda^i}{2}\frac{\lambda^j}{2}]\ (\epsilon.p)(\epsilon'.p)\delta_{ab} \tag{16}$$

(C) stop exchange in the u-channel:

$$A_{ab}^{Born\ C} = -\frac{16\pi\alpha_s}{u-m_{\widetilde{t}_a}^2}\ [\frac{\lambda^j}{2}\frac{\lambda^i}{2}]\ (\epsilon.p)(\epsilon'.p)\delta_{ab} \tag{17}$$

(we have used $\epsilon'.p' = -\epsilon'.p$ and $\epsilon.p' = -\epsilon.p$).

As one sees the Born terms only involve 2 invariant forms

$$I_1 = (\epsilon.p)(\epsilon'.p) \qquad I_2 = (\epsilon.\epsilon') \tag{18}$$

(and 4 color components, $C = 1, 4$), so that writing the invariant amplitude as

$$A = N_1(s,t,u)I_1 + N_2(s,t,u)I_2 \tag{19}$$

the helicity amplitudes are given by:

$$F_{\lambda_g,\lambda'_g} = -\frac{1}{2}\lambda_g\lambda'_g p^2 \sin^2\theta\ N_1(s,t,u) + \frac{1}{2}(1+\lambda_g\lambda'_g)\ N_2(s,t,u) \tag{20}$$

From Eqs. (10,12) and (20) one obtains the polarized Born cross sections

$$\frac{d\sigma^{Born}(\lambda_g,\lambda_g)}{d\cos\theta} = \frac{\pi\alpha_s^2\beta}{24s}(\ \frac{m_{\widetilde{t}_a}^4}{s^2}\ )[\ \frac{28+36\beta^2\cos^2\theta}{(1-\beta^2\cos^2\theta)^2}\ ] \tag{21}$$

$$\frac{d\sigma^{Born}(\lambda_g,-\lambda_g)}{d\cos\theta}=\frac{\pi\alpha_s^2\beta^5}{384s}[\ \frac{28+36\beta^2\cos^2\theta}{(1-\beta^2\cos^2\theta)^2}\ ]\sin^4\theta \tag{22}$$

in agreement with the results of ref.[2],[3]. Note that, at this Born level, $\sigma^{Born}(++) = \sigma^{Born}(--)$ and $\sigma^{Born}(+-) = \sigma^{Born}(-+)$.

It is useful, for later discussions of one loop effects, to emphasize the energy and angular dependences of the two types of polarized cross sections which are illustrated in Figs.(6,7).

At low energy the dominant cross sections are the so-called, [5], Gauge Boson Helicity Violating (GBHV) ones $\sigma(++,--)$ of Eq. (21). This arises because the invariant form I_2 has no threshold suppression factor, contrarily to I_1 which vanishes like β^2 near threshold. However at high energy the GBHV cross sections become mass suppressed like $m^4_{\widetilde{t}_a}/s^2$, as one can check from Eq. (21), in agreement with the general HC rule of ref.[5]. Consequently, as one sees in Fig. (6), between threshold ($2m_{\widetilde{t}_a}$) and about $3m_{\widetilde{t}_a}$, the stop pair is essentially produced through $\sigma(++,--)$, whereas for higher energies ($\sqrt{s} > 3m_{\widetilde{t}_a}$) it is dominated by the GBHC cross sections ($\sigma(+-,-+)$ of Eq. (22). In Fig.(7) we have shown the corresponding angular distributions which appear to be also totally different in the two cases, larger for central angles in $\sigma(+-,-+)$, see Eq. (22), as opposed to forward and backward peaks in $\sigma(++,--)$, Eq. (21). These various features will be essential for understanding the sensitivity to one loop effects in this process at LHC.

The stop pair can also be produced through the $q\bar{q}$ channel, Fig. (8), with a cross section

$$\frac{d\sigma}{d\cos\theta}=\frac{\pi\alpha_s^2\beta^3}{18s}\sin^2\theta \tag{23}$$

However, at LHC, this process is depressed as compared to the gluon-gluon one because of the smaller quark PdF's, so that there is no need to consider its one loop corrections.

III. ONE LOOP ELECTROWEAK CONTRIBUTIONS TO $g\,g\to\widetilde{t}_a\,\widetilde{t}^*_b$

The one loop electroweak contributions come from counter terms (c.t.) and self-energy (s.e.) corrections to the Born terms, and from triangle and box diagrams. We use the on-shell scheme [6] writing first the c.t.+s.e. corrections as:

For $a = b$:

$$A^{Born+c.t.+s.e.\ A}_{aa} \ = \ A^{Born\ A}_{aa}[1+\delta Z_{aa}] \tag{24}$$

$$A^{Born+c.t.+s.e.\ A'}_{aa} \ = \ A^{Born\ A'}_{aa}[1+\delta Z_{aa}] \tag{25}$$

$$A_{aa}^{Born+c.t.+s.e.\ B} = A_{aa}^{Born\ B}[1 + 2\delta Z_{aa} - \frac{\hat{\Sigma}_{aa}(t)}{t - m^2_{\widetilde{t}_a}}] \tag{26}$$

$$A_{aa}^{Born+c.t.+s.e.\ C} = A_{aa}^{Born\ C}[1 + 2\delta Z_{aa} - \frac{\hat{\Sigma}_{aa}(u)}{u - m^2_{\widetilde{t}_a}}] \tag{27}$$

and for $a \neq b$, using $A_{aa}^{Born\ A,A'} = A_{bb}^{Born\ A,A'}$

$$A_{ab}^{Born+c.t.+s.e.\ A} = A_{aa}^{Born\ A}\overline{\delta Z_{ba}} \tag{28}$$

$$A_{ab}^{Born+c.t.+s.e.\ A'} = A_{aa}^{Born\ A'}\overline{\delta Z_{ba}} \tag{29}$$

$$A_{ab}^{Born+c.t.+s.e.\ B} = A_{aa}^{Born\ B}[\overline{\delta Z_{ba}} - \frac{\hat{\Sigma}_{ab}(t)}{2(t - m^2_{\widetilde{t}_b})}] + A_{bb}^{Born\ B}[\overline{\delta Z_{ba}} - \frac{\hat{\Sigma}_{ab}(t)}{2(t - m^2_{\widetilde{t}_a})}] \tag{30}$$

$$A_{ab}^{Born+c.t.+s.e.\ C} = A_{aa}^{Born\ C}[\overline{\delta Z_{ba}} - \frac{\hat{\Sigma}_{ab}(u)}{2(u - m^2_{\widetilde{t}_b})}] + A_{bb}^{Born\ C}[\overline{\delta Z_{ba}} - \frac{\hat{\Sigma}_{ab}(u)}{2(u - m^2_{\widetilde{t}_a})}] \tag{31}$$

with the c.t. terms expressed in terms of stops self-energies

$$\delta Z_{aa} = -[\frac{d\Sigma_{aa}(p^2)}{dp^2}]_{p^2=m^2_{\widetilde{t}_a}} \tag{32}$$

and for $a \neq b$

$$\delta Z_{ba} = \frac{2\Sigma_{ba}(m^2_{\widetilde{t}_a})}{m^2_{\widetilde{t}_b} - m^2_{\widetilde{t}_a}} \tag{33}$$

$$\overline{\delta Z_{ba}} = \frac{1}{2}[\delta Z^*_{ba} + \delta Z_{ab}] \tag{34}$$

the renormalized s.e. functions being given by

$$\hat{\Sigma}_{aa}(p^2) = \Sigma_{aa}(p^2) - \Sigma_{aa}(m^2_{\widetilde{t}_a}) - (p^2 - m^2_{\widetilde{t}_a})[\frac{d\Sigma_{aa}(p^2)}{dp^2}]_{p^2=m^2_{\widetilde{t}_a}} \tag{35}$$

and for $a \neq b$

$$\hat{\Sigma}_{ba}(p^2) = \Sigma_{ba}(p^2) + \frac{p^2 - m^2_{\widetilde{t}_b}}{m^2_{\widetilde{t}_b} - m^2_{\widetilde{t}_a}}\Sigma_{ba}(m^2_{\widetilde{t}_a}) + \frac{p^2 - m^2_{\widetilde{t}_a}}{m^2_{\widetilde{t}_a} - m^2_{\widetilde{t}_b}}\Sigma^*_{ab}(m^2_{\widetilde{t}_b}) \tag{36}$$

The needed $\Sigma(p^2)$ functions are obtained from the various $(\widetilde{q}V)$, $(\widetilde{q}H)$, $(q\chi)$ bubbles and from the gauge boson (V) and the 4-leg $(SS\widetilde{t}\widetilde{t})$ tadpoles depicted in Fig (2) .

Triangle and boxes corrections are shown in Fig (3,4,5). They affect respectively each sector (A), (A'), (B) and (C) appearing in the Born case. In the s-channel one finds "left" and "right" triangles and in the t- and u- channels one has "up" and "down" ones. Contributions of sector (C) are obtained from those of sector (B) by symmetrization rules for the 2 gluons: interchange of momenta, polarization vectors and colors $(p_g, \epsilon(\lambda_g), i)$ and $(p'_g, \epsilon'(\lambda'_g), j)$. The 3 types of boxes can be identified through their (clockwise) internal contents $(SSVS)$, $(qq\chi q)$ and $(SSHS)$ for sector (B), the above symmetrization rules giving the crossed sector (C); S refer to all possible scalar states.

These electroweak corrections can also be classified into:

- *gauge* terms due to internal exchanges of gauge bosons ($V = \gamma, Z, W$) and of charginos, neutralinos (through their gaugino components),
- *Yukawa* terms due to exchanges of Higgs bosons (H), and also charginos, neutralinos (now through their higgsino components).

The contributions of these various diagrams to the helicity amplitudes are obtained after color decomposition according to Eq. (9) and are expressed in terms of Passarino-Veltman (PV) functions. The numerical computation is then done with a dedicated c++ code exploiting the LoopTools library [8].

A first check of the computation is obtained by observing the cancellation of the divergences appearing in counter terms, self-energies, triangles and boxes. For some parts these cancellations occur separately in each sector, but for other parts they involve contributions from several sectors as required by gauge invariance.

Another type of check is provided by the high energy behavior of the helicity amplitudes which has to satisfy a number of "asymptotic" rules.

As already noticed in Sect.II, at high energy, neglecting masses the only surviving Born helicity amplitudes obtained from the addition of (A+A'+B+C) terms are the GBHC ones:

$$F^{Born}_{\lambda_g,\ -\lambda_g} = (4\pi\alpha_s)(\frac{\sin^2\theta}{2})[\frac{c_{ij}}{1-\cos\theta} + \frac{c'_{ij}}{1+\cos\theta}] \tag{37}$$

with

$$c_{ij} = \frac{1}{3}\delta^{ij} + d^{ijl}(\frac{\lambda^l}{2}) + if^{ijl}(\frac{\lambda^l}{2}) \qquad c'_{ij} = \frac{1}{3}\delta^{ij} + d^{ijl}(\frac{\lambda^l}{2}) - if^{ijl}(\frac{\lambda^l}{2}) \tag{38}$$

in agreement with the theorem given in [5], whereas the GBHV ones (with $\lambda_g = \lambda'_g$) are mass suppressed (vanish like m^2/s).

From the general logarithmic rules established in [7] , one expects the one loop virtual electroweak contributions to give, for final unmixed L, R states (before applying the mixing matrices R_{ai}), the following corrections to the GBHC Born amplitudes (M is the mass scale of the single logarithms and is beyond the accuracy of the expressions below):

$$F_{\lambda_g,\ -\lambda_g} = F^{Born}_{\lambda_g,\ -\lambda_g}[1 + c_{\widetilde{tt}}] \tag{39}$$

$$c_{\widetilde{t_L}\widetilde{t_L}} = \frac{\alpha(1+26c_W^2}{144\pi c_W^2 s_W^2}\left(2\log\frac{s}{M^2} - \log^2\frac{s}{M_W^2}\right) - \frac{\alpha(\widetilde{m}_t^2 + \widetilde{m}_b^2)}{8\pi s_W^2 M_W^2}\log\frac{s}{M^2} \tag{40}$$

$$c_{\widetilde{t_R}\widetilde{t_R}} = \frac{\alpha}{9\pi c_W^2}\left(2\log\frac{s}{M^2} - \log^2\frac{s}{M_W^2}\right) - \frac{\alpha\widetilde{m}_t^2}{4\pi s_W^2 M_W^2}\log\frac{s}{M^2} \tag{41}$$

$$\widetilde{m}_t = \frac{m_t}{\sin\beta} \qquad \widetilde{m}_b = \frac{m_b}{\cos\beta} \tag{42}$$

in which one identifies the "gauge" and the "Yukawa" parts.

We have checked analytically (by taking the leading logarithmic expressions of the PV functions) that the various self-energy, triangle and box contributions reproduce the above expressions in both gauge and Yukawa sectors.

We conclude this Section by briefly discussing the treatment of infrared singularities. As usual, QED radiation effects can be split into a soft part which is infrared (IR) singular and a hard part including the emission of photons with an energy which is not small compared to the process energy scale. In this paper, we have only included the soft part which is necessary in order to cancel any the IR singularities associated with the photonic virtual corrections.

We denote by $\mathcal{A}^{\rm Born}$ and $\mathcal{A}^{1\ \rm loop}$ any invariant helicity scattering amplitude evaluated at Born or one loop level. IR divergences are regulated by a small photon mass λ. IR cancellation holds for every helicity channel separately and we checked it numerically by

taking the $\lambda \to 0$ limit of our calculation. The real radiation factorizes on the Born amplitude leading to

$$\left(\mathcal{A}^{\rm Born}\right)^2 \left(1 + \frac{\alpha}{2\pi}\delta_s\right) + 2\mathcal{A}^{\rm Born}\ \mathcal{A}^{1\ \rm loop} = \text{IR finite.} \tag{43}$$

The universal correction factor δ_S takes into account the emission of soft real photons with energy from λ up to $\Delta E_\gamma^{\rm max} \ll \sqrt{s}$ [9]. In our analysis, we have fixed $\Delta E_\gamma^{\rm max} = 0.1$ GeV.

IV. RESULTS

Our starting observable for this process is the invariant mass distribution defined as

$$\begin{aligned}\frac{d\sigma(pp \overset{gg}{\to} \widetilde{t}_a\, \widetilde{t}_b^* + X)}{dM_{\rm inv}} &= \int dx_1\, dx_2\, d\cos\theta\, g(x_1,\mu)\, g(x_2,\mu) \\ &\times \frac{d\sigma_{gg\to \widetilde{t}_a\, \widetilde{t}_b^*}}{d\cos\theta}\, \delta(\sqrt{x_1 x_2 S} - M_{\rm inv})\,,\end{aligned} \tag{44}$$

where $\sqrt{S}$ is the proton-proton c.m. energy, $M_{\rm inv}$ is the $\widetilde{t}_a + \widetilde{t}_b^*$ invariant mass, θ is the stop squark scattering angle in the partonic c.m. frame, and $g(x_i,\mu)$ are the distributions of the gluon inside the proton with a momentum fraction x_i at the scale μ. We have used the LO PDF set CTEQ6L [11] with $\mu = m_{\widetilde{t}_a} + m_{\widetilde{t}_b}$. As we already mentioned, we include soft QED real radiation in order to cancel IR singularities. For the $2 \to 2 + \gamma(\text{soft})$ process we can identify $M_{\rm inv}$ with the partonic c.m. energy $\sqrt{s}$. The shift induced by hard QCD radiation has been previously estimated for $t\,\overline{t}$ production in [10] and found to be at the level of a few percents. Since our observables will be defined by integrating over a wide range of $M_{\rm inv}$ values, such a shift will be irrelevant for our conclusions.

For our purposes, we have first considered the total rate $\sigma_{\rm tot}$ of the process defined by integrating the distribution $d\sigma/dM_{\rm inv}$ over the full range of invariant mass values, from the threshold $m_{\widetilde{t}_a} + m_{\widetilde{t}_b}$, for the diagonal light squark production $(\widetilde{t}_1\widetilde{t}_1^*)$ and for the non-diagonal case $(\widetilde{t}_1\widetilde{t}_2^* + \widetilde{t}_2\widetilde{t}_1^*)$. For the diagonal process we have considered a quantity that we call *partial rate* and is defined as follows

$$\sigma(M_{\rm inv}) = \int_{M_{\rm inv}}^{\infty} \frac{d\sigma}{dM'_{\rm inv}}\, dM'_{\rm inv}. \tag{45}$$

Note that our definition must not be confused with that of the conventional partial decay rates. In our definition *partial* refers to the constrained integration range.

Our analysis has been performed for a choice of 10 SUSY benchmark points. More specifically, we have considered the six SPS points SPS 1-6 [12], the two SU1, SU6 ATLAS points [4] and two additional light SUSY scenarios LS1 and LS2 discussed in [13].

Our results are shown in the next Figures. We have tried to draw a limited number of curves, that contain all the information that seems more relevant to us. With this purpose, we have first shown in Figs.(9,10) the shape of the differential distribution $d\sigma/dM_{\rm inv}$ with the related relative effect for two representative points, chosen as LS1 and SPS5. One notices that a positive relative effect is present in the very low mass region, that soon vanishes and becomes negative approaching typically a -10% limit. The same feature persists in all the remaining considered points. This can be understood from the discussion of the various helicity amplitudes in Sec. (II). At large $M_{\rm inv}$, the helicity conserving amplitude dominates with its Sudakov negative correction, while at small $M_{\rm inv}$ the helicity violating amplitude is the larger one and receives a positive correction in a narrow region near the production threshold. As a consequence one may expect to find a rather small effect in the total rate due to the cancellation between the corrections in these two regimes, but a non negligible negative effect if the integration limit of the partial rates is sufficiently large.

With this purpose, we have first shown in Figs.(11,12) a number of *partial rates*, defined by Eq. (45), drawn at variable initial invariant mass integration limit. From these figures, one can read the value of the total rate that corresponds to the physical threshold. Also, for each choice of $M_{\rm inv}$ one can see the value of the corresponding partial rate and the relative one-loop effect (lower curves). In this way, one can visualize for each $M_{\rm inv}$ the correspondence between a certain percentage effect and the related value of the partial rate.

In Fig. (11) we have displayed the results obtained for the two *light SUSY* points LS1, LS2 for which (as for all the other benchmark points) Tab. (I) contains the MSSM parameter values. As one sees, the values of our total electroweak rate is of 27 and 22 pb respectively (note that all the values that we obtained for the various rates do not contain the NLO QCD effects, that roughly speaking multiply the electroweak rate by a factor $\simeq 1.4$ [1]). One sees that the overall one-loop effect is rather small (a fraction of a percent). Raising the integration limit, the value of the rate decreases, but the relative one-loop electroweak effect increases. If we consider 1 pb as a realistic observability limit for the rates, we conclude that for a value of $M_{\rm inv}$ of approximately 1.2 TeV a relative effect of 10 % on the partial rate would be present for both benchmark points.

Fig. (12) shows the results for two *heavy stop* points that still exhibit realistically measurable values of the total and partial rates, *i.e.* SPS5 and SPS1. For the first one the lowest limit of 1 pb, obtained for $M_{\rm inv} \simeq 1$ TeV, shows a relative one-loop effect of approximately 8%. For SPS1 again at $M_{\rm inv} \simeq 1$ TeV, a relative effect of approximately 5% would appear.

In Tab. (II) we have reported the values of the total rates of the last six considered benchmark points. As one sees, the rates for all these points are rather small (0.2 pb or less) and a search of relative one-loop effects would be, in our opinion, rather academic.

In conclusion, it seems to us that for only four of the 10 selected benchmark points an experimental determination would be, a priori, realistically performable in the first LHC runs. Still, for completeness, we have tried to make a comparison of the different relative SUSY effects for all 10 benchmark points, using as input parameter the value of the light stop mass at the various points. In Fig. (13) we have shown, for all points, the relative electroweak one-loop effects that one would find by considering first the various total rates, and secondly the partial rates that would correspond to an integration from $3\, m_{\widetilde{t}_1}$ to infinity (this choice is purely indicative). The main features that arise from Fig. (13) are:

1. In all cases, the relative effect on the total rate is rather small, a few percent at most.

2. In all cases, the relative effect on the partial rates $\sigma(3\, m_{\widetilde{t}_1})$ is sizeable and negative, varying from approx. -6 % to -10 % in the various cases. In particular one sees that for the four *realistic* benchmark points, a dedicated experimental effort might succeed in detecting the associated virtual effects that, we remind, correspond to relatively light ($\lesssim 300$ GeV) $\widetilde{t}_1$ masses.

At this point of our analysis, a general comment can be devoted to the differences between the various relative effects in the considered models. In more details, if one considers the two points SPS3 and SPS5 for which the $\widetilde{t}_1$ mass is drastically different (645 and 279 GeV) one sees that the relative effect is identical. On the contrary, the pair of points SPS6 and SPS4 have very similar $\widetilde{t}_1$ masses but quite different $\tan\beta$ (10 and 50) and the effect is appreciably different (from -7% to -10%). In a *Sudakov based* approach, the larger values of $\tan\beta$ would indeed produce a larger negative shift coming from the Yukawa couplings. In the case of LS1 and LS2, for which the same difference in $\tan\beta$ exists, the integration energies are smaller and this Sudakov dominance argument is reduced.

We have also computed, for all benchmark points, the non diagonal total rate derived from one-loop gg electroweak diagrams. We remind the reader that a calculation of the non diagonal rate, derived from $q\overline{q}$ annihilation at Born level via Z exchange, already exists [2] for SPS5. The value that is obtained is larger than that coming from the kinematically depressed NLO QCD diagrams, and is equal to $\simeq 6 \cdot 10^{-4}$ pb. In Tab. (III), we show the values that we have derived for the different benchmark points both for the one-loop gg diagrams and from the Z exchange calculations. One sees that the one-loop electroweak values are of the same size as those due to Z exchange and in some cases larger. This could have some relevance for the four *meaningful* benchmark points. For example, in the LS2 case, summing the one-loop with the Z-exchange contribution, one would get a total rate of approximately 10^{-2} pb. This is a factor 15 larger than the SPS5 point of [2], and might lead to experimental detection. In this spirit, we show only for this case in Fig. (14) the detailed invariant mass distribution. A similar slightly weaker conclusion might be drawn for the rates of the three remaining points if one sums the one-loop with the Z-exchange contributions.

V. CONCLUSIONS

We have devoted our analysis to the search of possibly observable electroweak one-loop effects in the process of light stop - antistop production at LHC. With this purpose we have only considered the one-loop effects on the largely dominant gg initiated channel. Having chosen a set of 10 representative SUSY benchmarks, we have seen that for only four of them the total production rate would be above the 1 pb limit, being practically unaffected by one-loop contributions. A better chance for these corrections would be provided by the measurements of partial rates, for which relative negative effects not far from the 10% size would be produced. These effects have been illustrated for all the 10 benchmark points. Although the rigorous dependence on the different SUSY parameters is difficult to display, a qualitative enhancement with large $\tan\beta$ seems to be confirmed, as expected in a Sudakov limit from the squarks Yukawa couplings. For the non diagonal rates we have found one-loop values that, summed with those coming from the single Z-exchange, might be, in a hopefully large luminosity stage, in principle observable.

At the moment of concluding this work, we became aware of a preprint that just appeared

from Hollik, Kollar and Trenkel. This contains a one-loop electroweak analysis for diagonal production performed for 4 benchmark points which gives the total rates including the QCD and QED effects, in particular the *NLO QED* contribution coming from the initial $\gamma\, g$ state. This appears to be an interesting analysis, complementary to the search of virtual effects that we have presented here where we have tried to identify suitable observables and to understand a possible dependence of the effects on SUSY parameters different from the stop masses. Certainly, a detailed comparison with our results would be welcome.

---

[1] W. Beenakker, M. Kramer, T. Plehn, M. Spira and P. M. Zerwas, Nucl. Phys. B **515**, 3 (1998) [arXiv:hep-ph/9710451].

[2] G. Bozzi, B. Fuks and M. Klasen, Phys. Rev. D **72**, 035016 (2005) [arXiv:hep-ph/0507073].

[3] T. Gehrmann, D. Maitre and D. Wyler, Nucl. Phys. B **703**, 147 (2005)

[4] ATLAS Data Challenge 2 DC2 points:
`http://paige.home.cern.ch/paige/fullsusy/romeindex.html`.

[5] G.J. Gounaris and F.M. Renard, Phys. Rev. Lett. 94,131601,2005, hep-ph/0501046; Addendum in Phys. Rev. D D73,097301,2006, hep-ph/0604041.

[6] W.F.L. Hollik, Fortsch. Physik **38**:165(1990).

[7] M. Beccaria, F.M. Renard and C. Verzegnassi, hep-ph/0203254; *Logarithmic Fingerprints of Virtual Supersymmetry*, Linear Collider note LC-TH-2002-005, GDR Supersymmetrie note GDR-S-081.

M. Beccaria, M. Melles, F. M. Renard, S. Trimarchi, C. Verzegnassi, Int. Jour. Mod. Phys.**A18**,5069,2003, hep-ph/0304110.

[8] T. Hahn and M. Perez-Victoria, Comput. Phys. Commun. **118**, 153 (1999) [arXiv:hep-ph/9807565].

[9] G. 't Hooft and M. J. G. Veltman, Nucl. Phys. B **153**, 365 (1979).

[10] M. Beccaria, S. Bentvelsen, M. Cobal, F. M. Renard and C. Verzegnassi, Phys. Rev. D **71**, 073003 (2005) [arXiv:hep-ph/0412249].

[11] J. Pumplin, D. R. Stump, J. Huston, H. L. Lai, P. Nadolsky and W. K. Tung, JHEP **0207**, 012 (2002) [arXiv:hep-ph/0201195].

[12] B. C. Allanach *et al.*, *The Snowmass points and slopes: Benchmarks for SUSY searches*, in

Proc. of the APS/DPF/DPB Summer Study on the Future of Particle Physics (Snowmass 2001) ed. N. Graf, *In the Proceedings of APS / DPF / DPB Summer Study on the Future of Particle Physics (Snowmass 2001), Snowmass, Colorado, 30 Jun - 21 Jul 2001, pp P125* [arXiv:hep-ph/0202233].

[13] M. Beccaria, G. Macorini, F. M. Renard and C. Verzegnassi, Phys. Rev. D **74**, 013008 (2006) [arXiv:hep-ph/0605108].

[14] T. Gehrmann, D. Maitre and D. Wyler, Nucl. Phys. B **703**, 147 (2004) [arXiv:hep-ph/0406222].

mSUGRA scenario	m_0	$m_{1/2}$	A_0	$\tan\beta$	sign μ
LS1	300	150	-500	10	+
LS2	300	150	-500	50	+
SPS1	100	250	-100	10	+
SPS2	1450	300	0	10	+
SPS3	90	400	0	10	+
SPS4	400	300	0	50	+
SPS5	150	300	-1000	5	+
SPS6	150	300	0	10	+
SU1	70	350	0	10	+
SU6	320	375	0	50	+

TABLE I: mSUGRA benchmark points

	$\sigma_{gg\to\tilde{t}_1\tilde{t}_1^*}$
LS1	27.35
LS2	22.08
SPS5	7.57
SPS1	1.12
SPS6	0.33
SPS4	0.198
SU1	0.15
SU6	0.075
SPS3	0.067
SPS2	0.0063

TABLE II: Total cross-sections (in pb) for diagonal stop production.

	$\sigma_{q\bar{q}\to\tilde{t}_1\tilde{t}_2^*+\tilde{t}_2\tilde{t}_1^*}$	$\sigma_{gg\to\tilde{t}_1\tilde{t}_2^*+\tilde{t}_2\tilde{t}_1^*}$
LS2	0.0034	0.0058
LS1	0.0026	0.0013
SPS5	0.00057	0.00053
SPS1	0.00054	0.00038
SPS6	0.00022	0.00013
SPS4	0.00017	0.00045
SU1	0.00011	0.000057
SU6	0.000081	0.00016
SPS3	0.000057	0.000024
SPS2	0.00000044	0.00000023

TABLE III: Total cross-sections (in pb) for non-diagonal stop production starting from $q\bar{q}$ and gg.

Tree diagrams

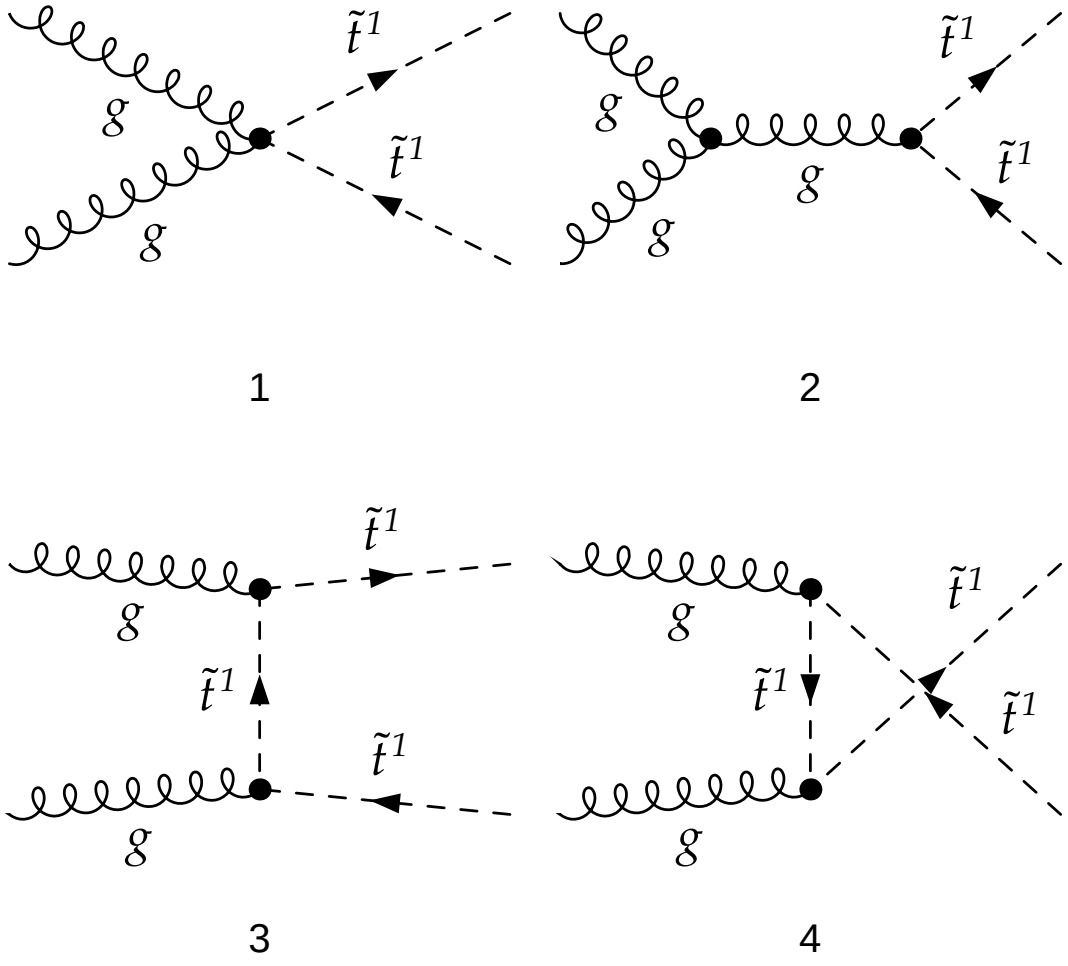

FIG. 1: Tree level diagrams for diagonal production $g\,g \to \bar{t}_1\,\bar{t}_1^*$.

s.e. diagrams

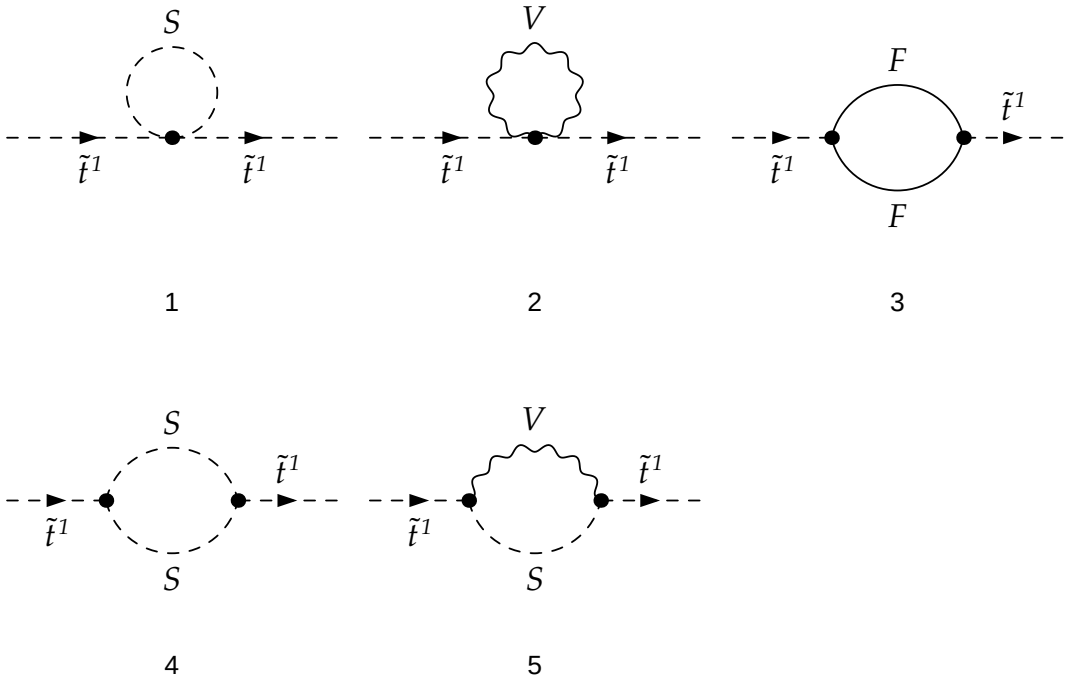

FIG. 2: Self-energy (generic) diagrams for diagonal production $g\,g \to \overline{t}_1\,\overline{t}_1^*$. They are composed of: scalar and vector tadpoles where the particles can be higgs bosons, sleptons and squarks (1) and SU(2)×U(1) gauge bosons (2); scalar, fermion and scalar-vector bubbles where the particles can be quark-χ (3), squark-higgs (4) and squark-e.w. gauge boson (5).

up/down/left/right triangles

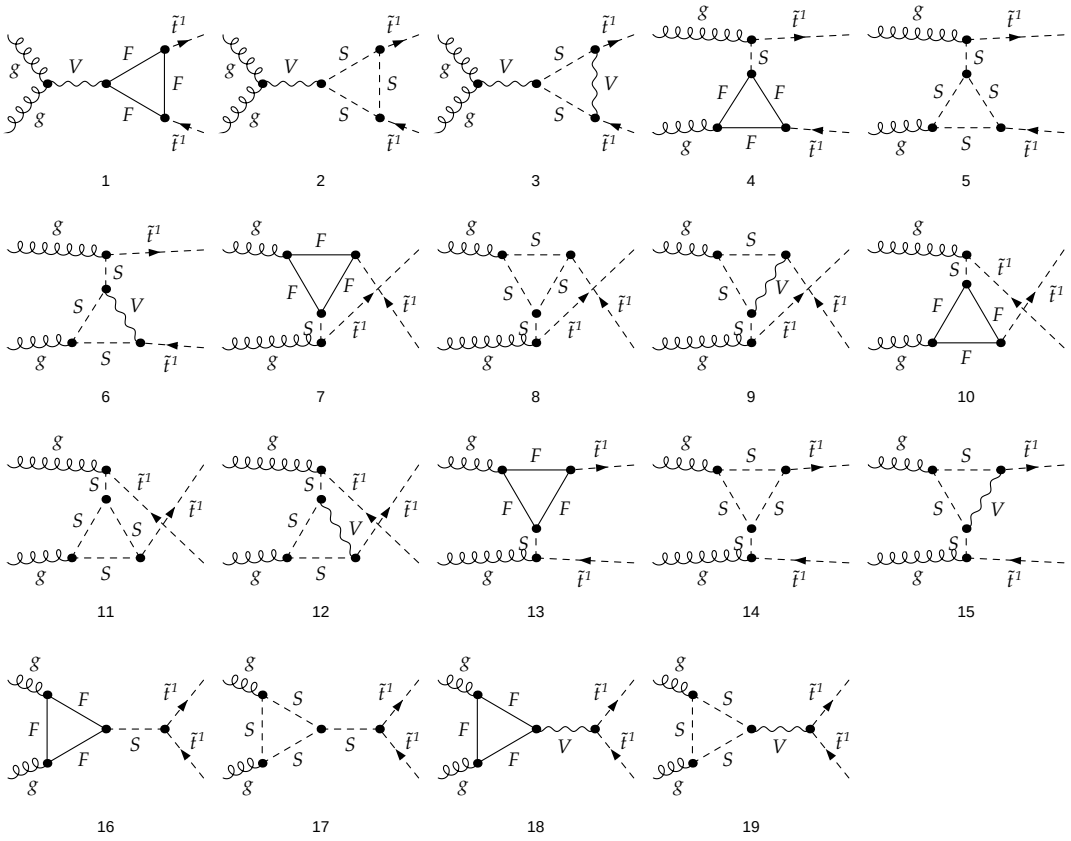

FIG. 3: Up, down, left and right triangle (generic) diagrams for diagonal production $g\,g \to \overline{t}_1\,\overline{t}_1^*$. In the s-channel diagrams (1), (2), (3) we have labelled the internal gluon as a generic vector, while all the other vector particles are intended to be SU(2)×U(1) gauge bosons. Fermion loops and scalar loops involve quarks-χ and squarks-higgs respectively, with the exception of diagrams (16), (17), (18) and (19) where the loops involve only quarks and squarks.

4 legs triangles

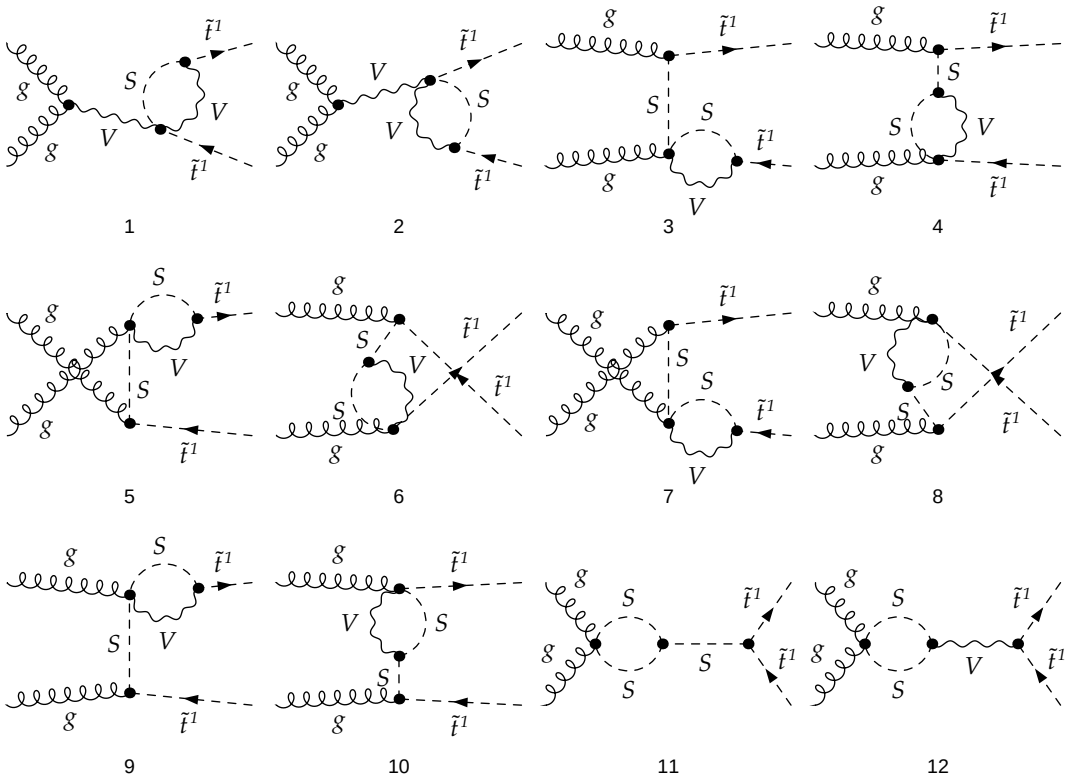

FIG. 4: Four legs triangle (generic) diagrams for diagonal production $g\,g \to \overline{t}_1\,\overline{t}_1^*$. As in the previous figure we label s-channel internal gluons in diagrams (1) and (2) as vectors, while all the other vectors are e.w. gauge bosons. The s-channel scalar in diagram (11) can be any neutral higgs.

Boxes

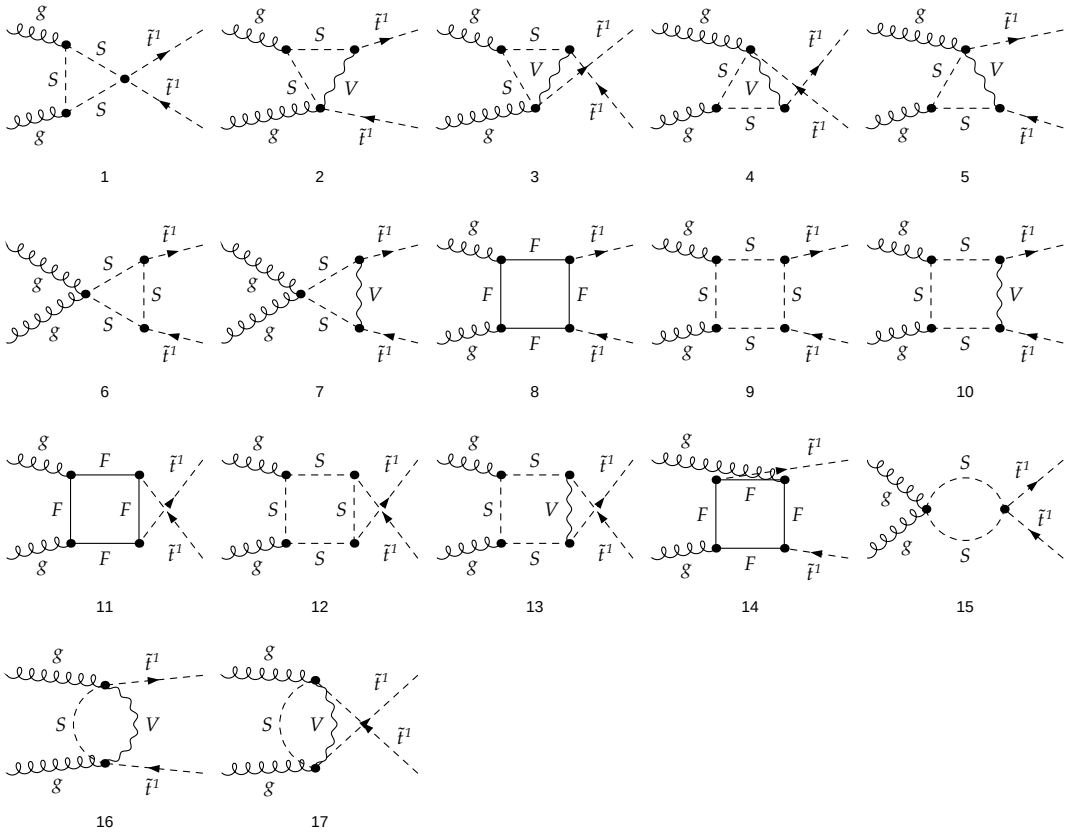

FIG. 5: Box (generic) diagrams for diagonal production $g\,g \to \overline{t}_1\,\overline{t}_1^*$. Every vector is an e.w. gauge boson; 4-fermions boxes are made of 3 quarks and a χ; 4-scalars boxes are made of 3 squarks and a higgs boson.

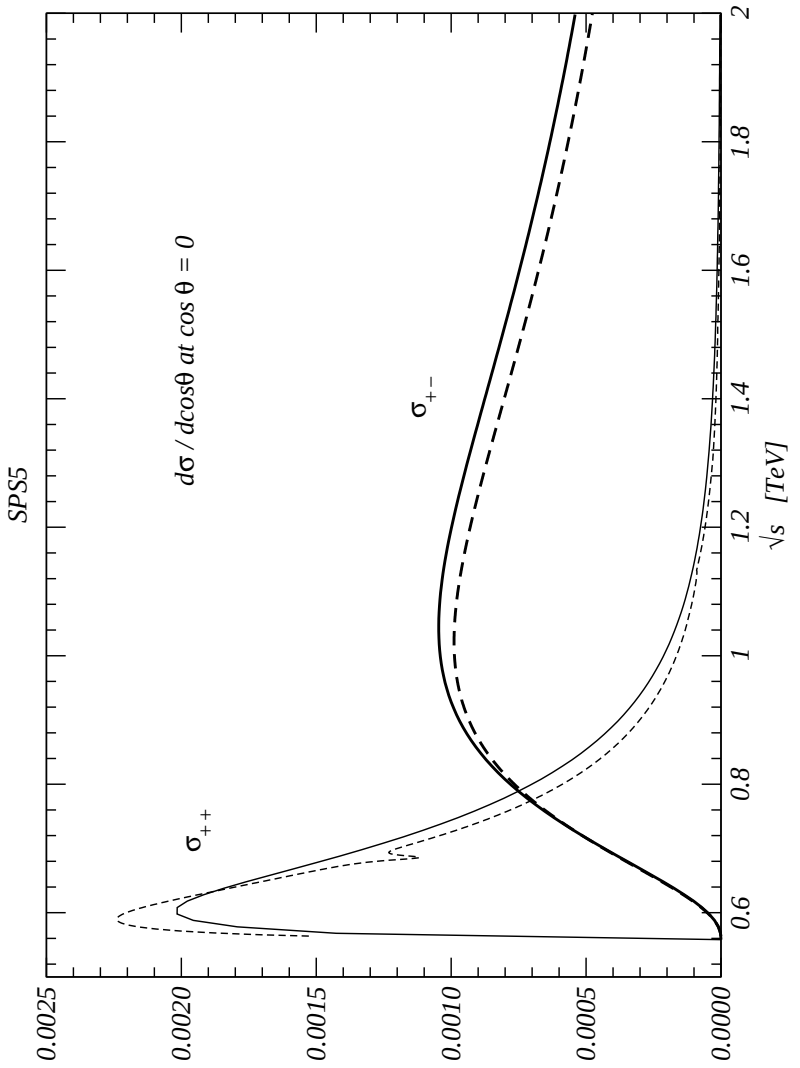

FIG. 6: Differential cross section at parton level. Energy dependence at fixed angle of the helicity violating (++) and conserving (+-) components. The dashed lines include the one-loop corrections.

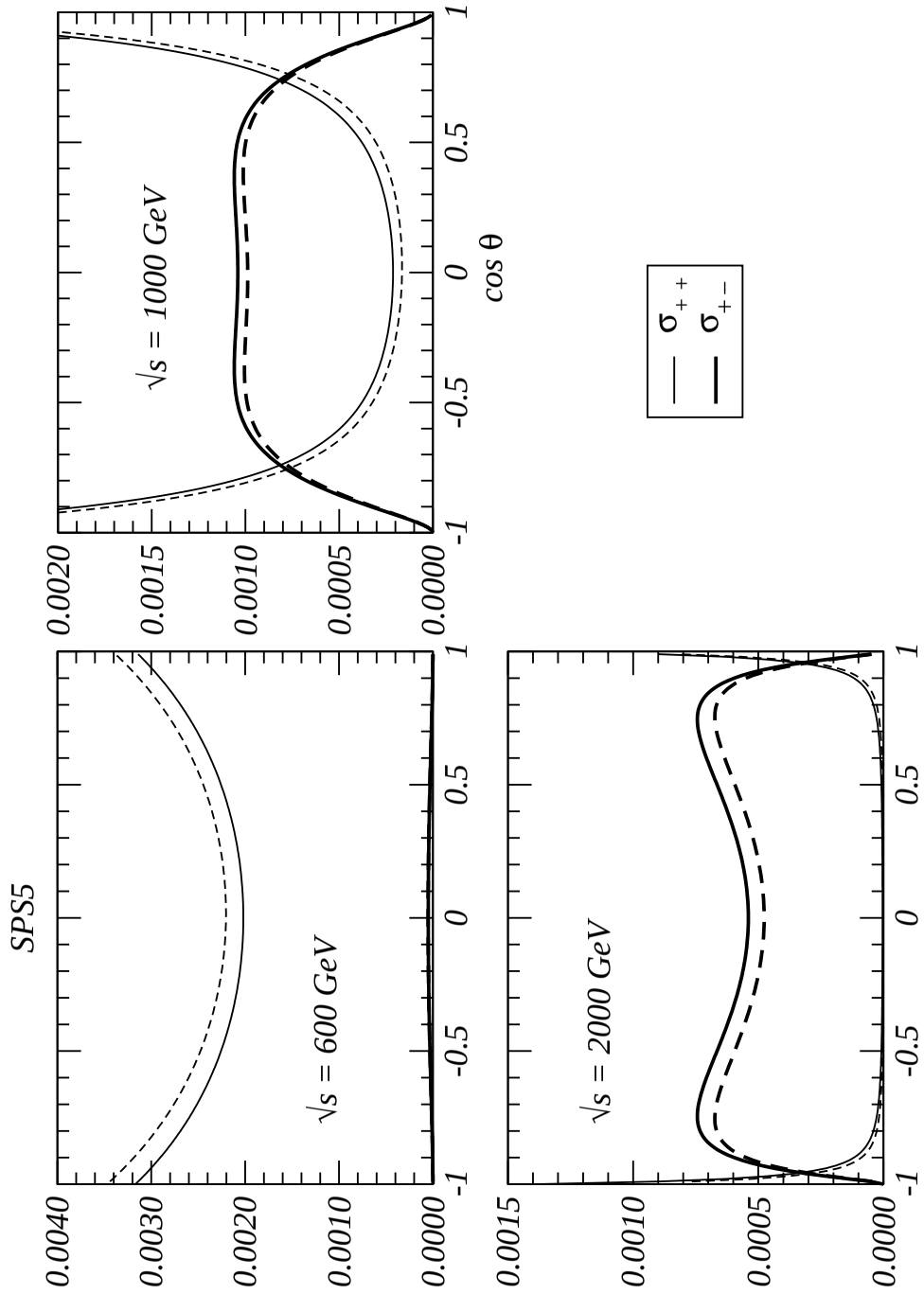

FIG. 7: Differential cross section at parton level. Angular dependence of the helicity violating (++) and conserving (+-) components. The dashed lines include the one-loop corrections.

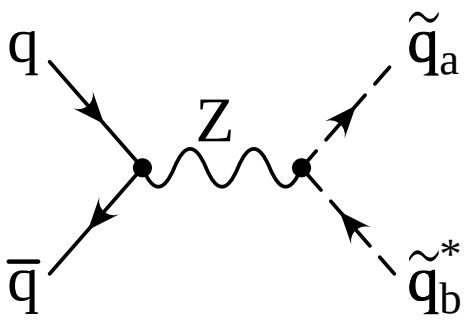

FIG. 8: Born diagram for non-diagonal squark production $q\,\overline{q} \to \widetilde{t}_a\,\widetilde{t}^*_b$, $(a \neq b)$, via Z boson exchange.

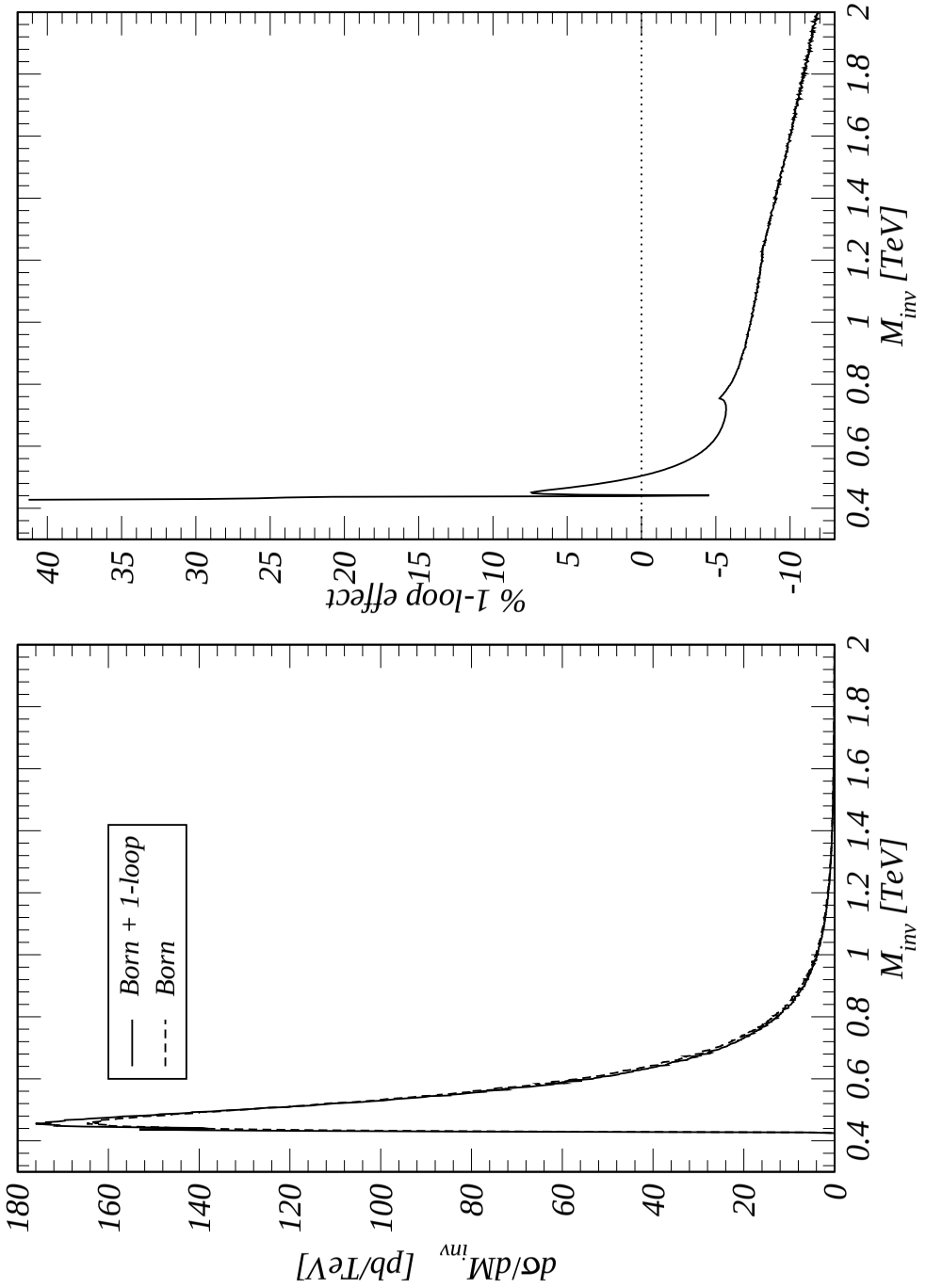

FIG. 9: LS1, Born and one-loop distribution $d\sigma/dM_{\rm inv}$. The right panel shows the percentual relative effect.

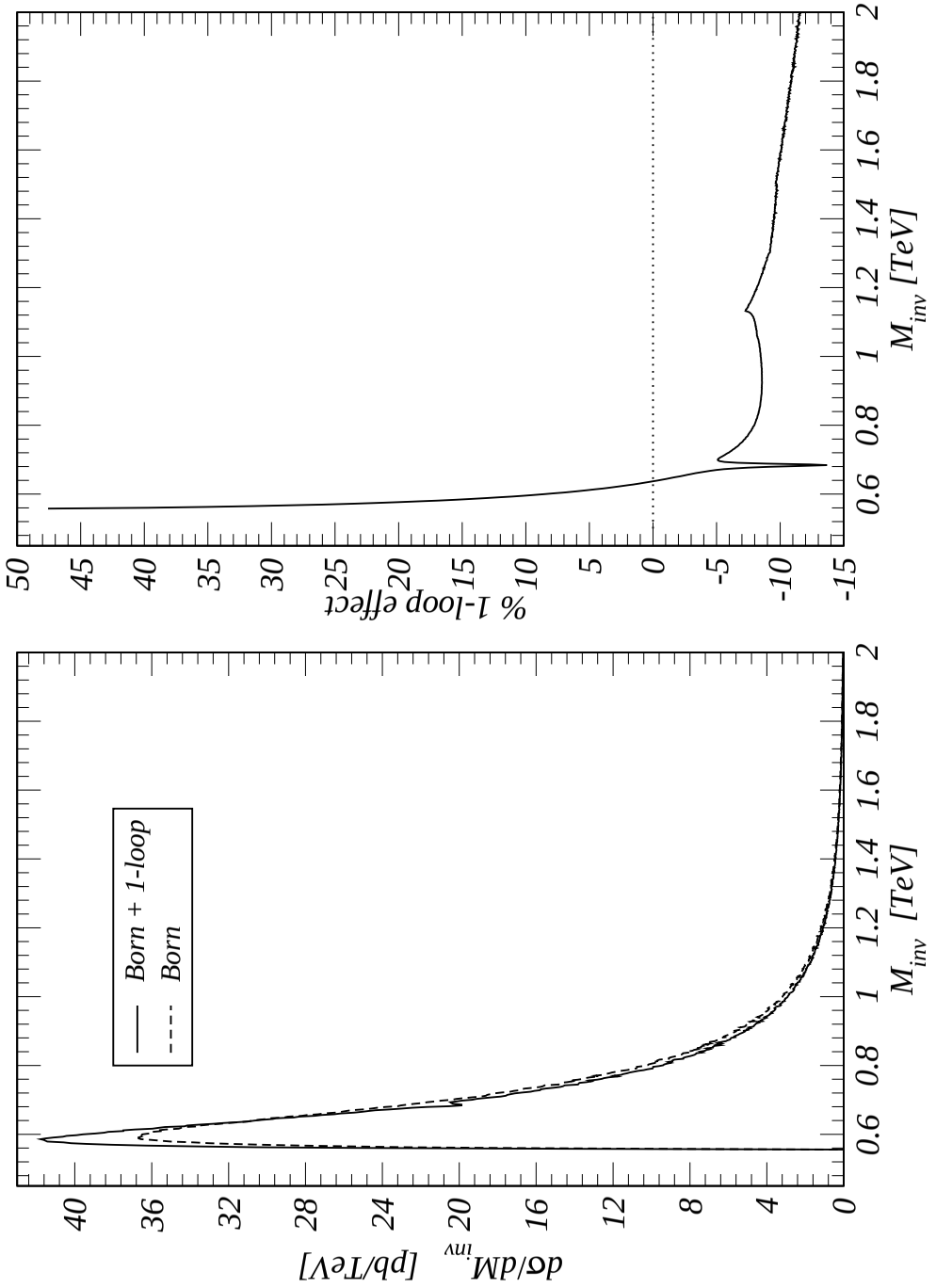

FIG. 10: SPS5, Born and one-loop distribution $d\sigma/dM_{\rm inv}$. The right panel shows the percentual relative effect.

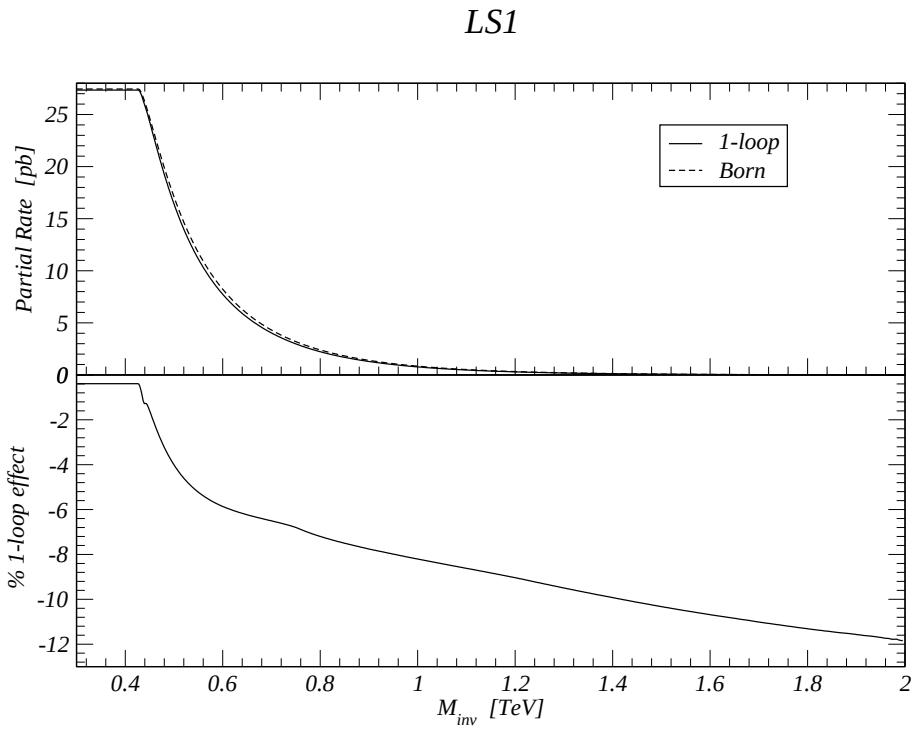

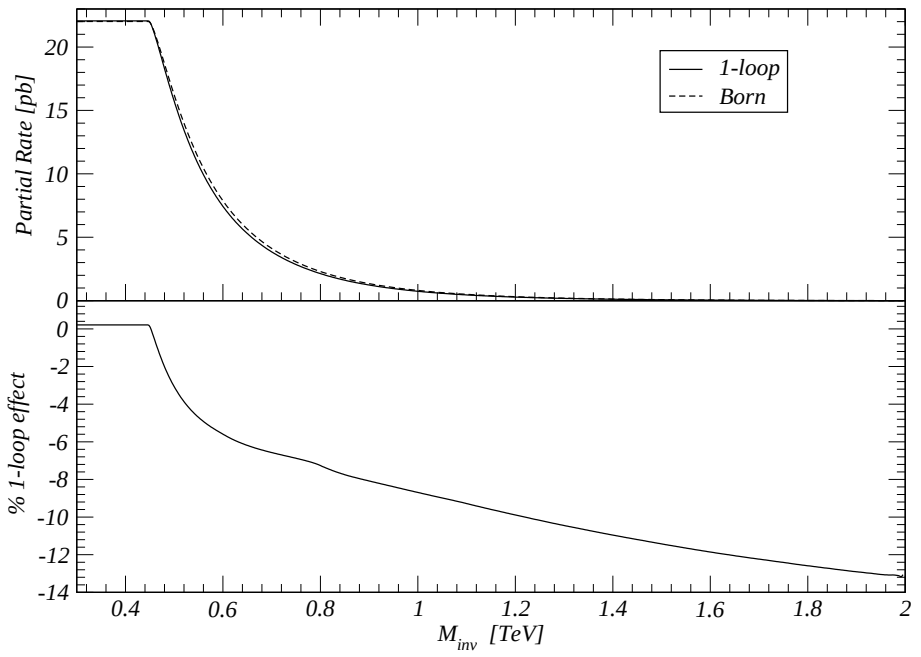

FIG. 11: LS1, LS2, partial rate $\sigma(M_{\rm inv})$ and one-loop effect.

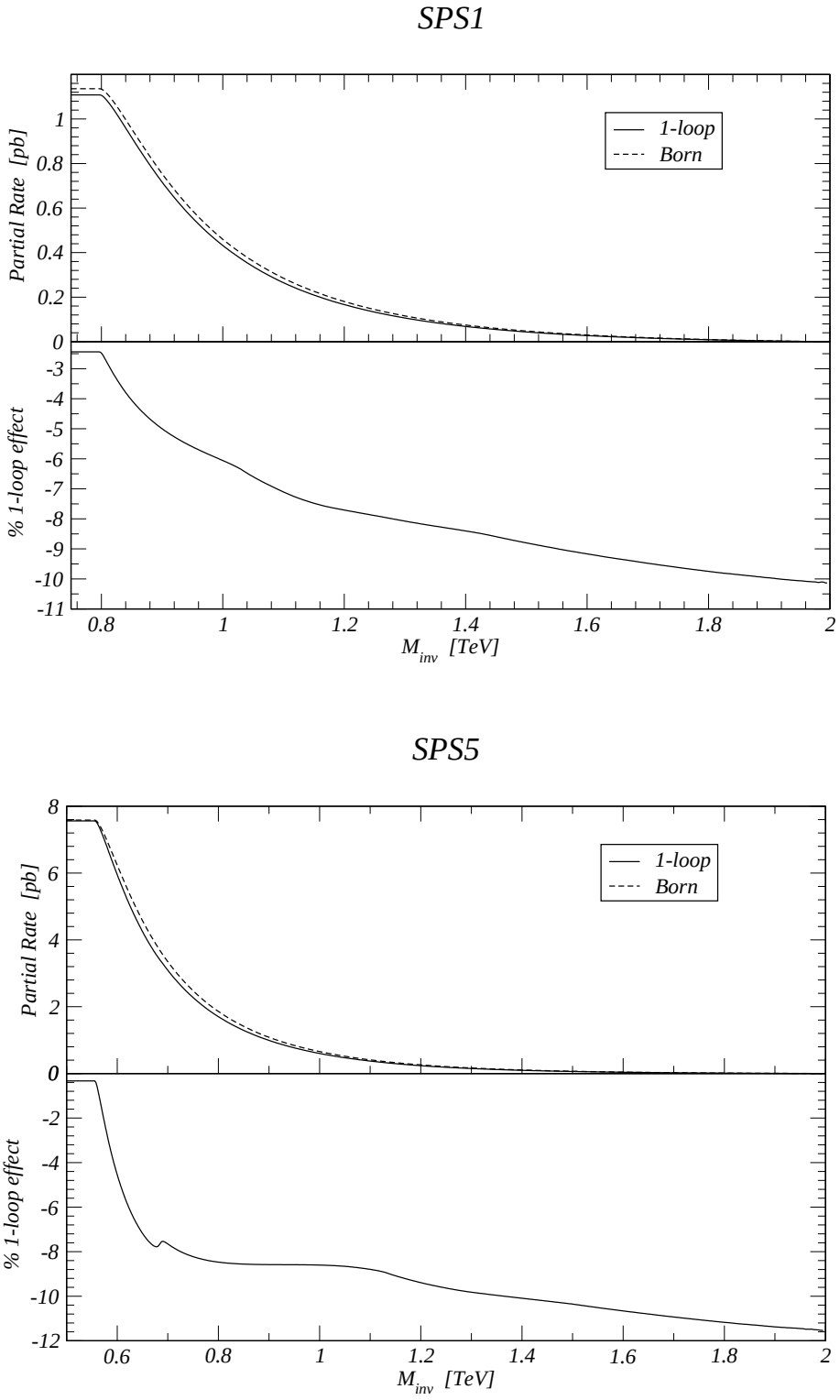

FIG. 12: SPS1, SPS5, partial rate $\sigma(M_{\rm inv})$ and one-loop effect.

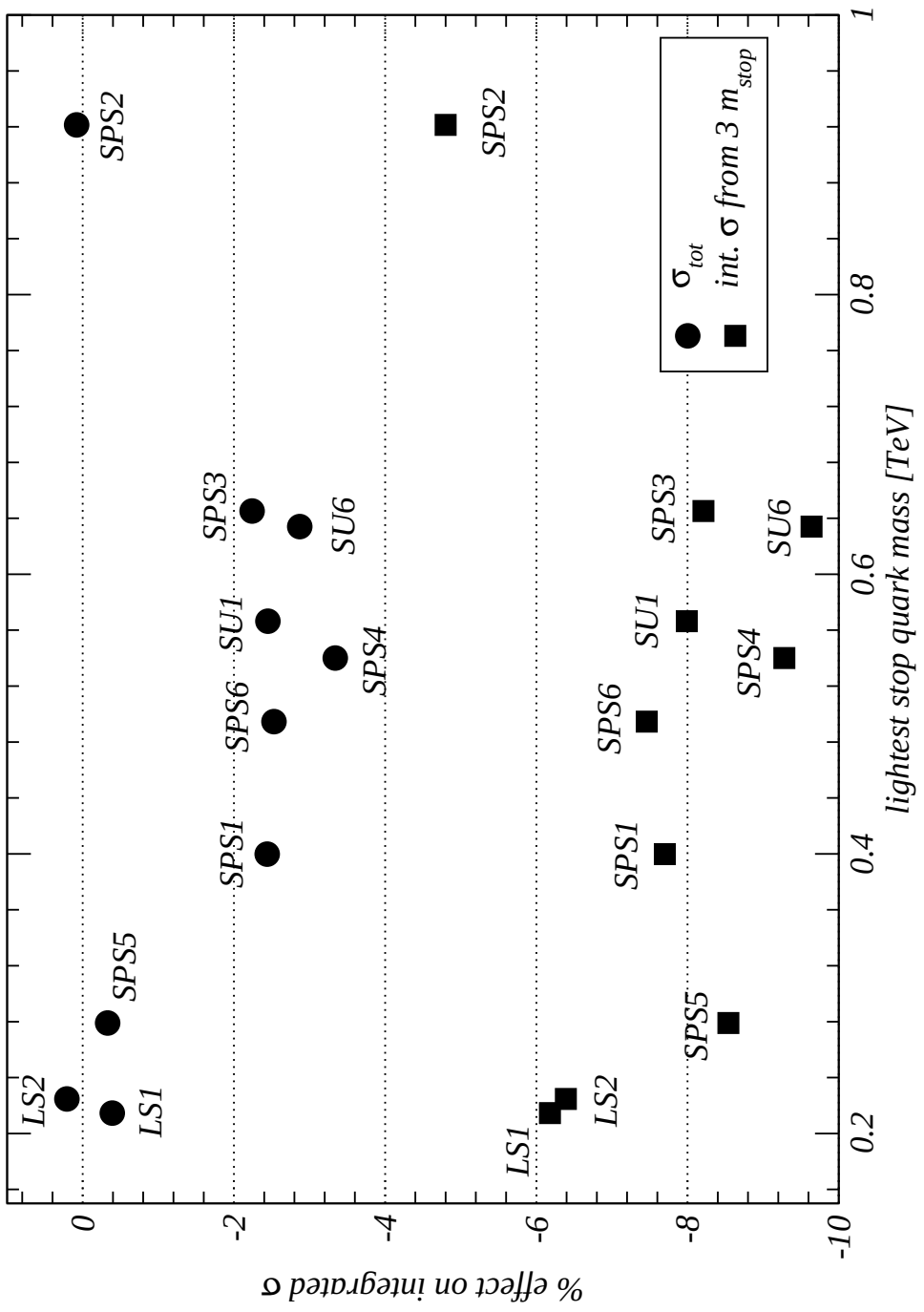

FIG. 13: Summary plot showing for the 10 benchmarks points the electroweak one-loop effect on the total cross section (circles) and on the partial rate obtained integrating $d\sigma/dM_{\rm inv}$ from $3\,m_{\tilde{t}_1}$ to infinity (squares).

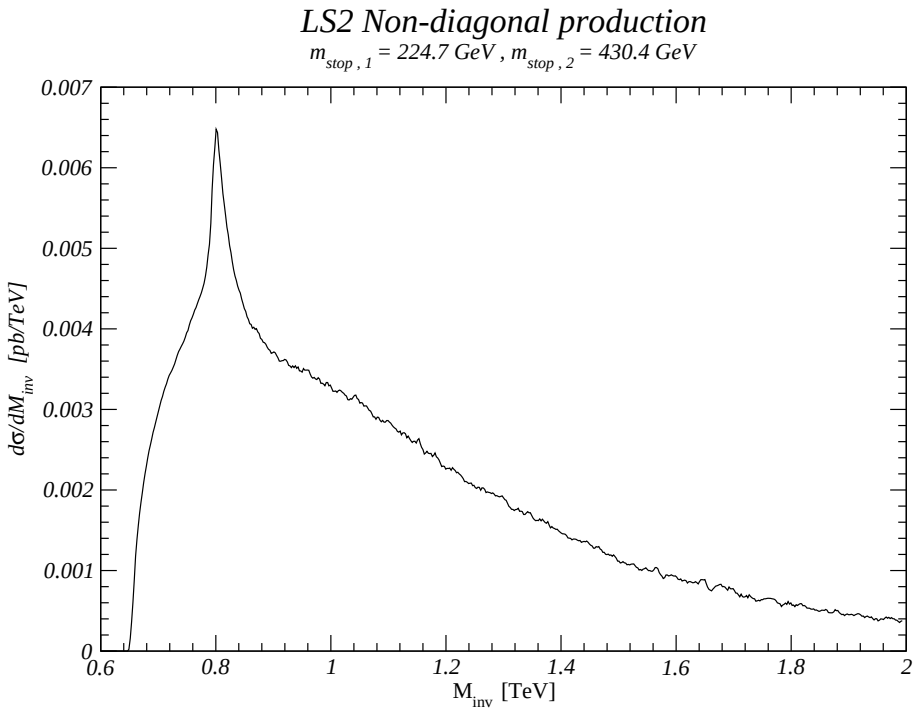

FIG. 14: LS2, non diagonal distribution $d\sigma/dM_{\rm inv}$.